Antiferrodistortive phase transition in pseudorhombohedral $(Pb_{0.94}Sr_{0.06})(Zr_{0.550}Ti_{0.450})O_3$: A combined synchrotron x-ray and neutron powder diffraction study

Ravindra Singh Solanki,[1] S. K. Mishra,[2] Anatoliy Senyshyn,[3] I. Ishii,[4] Chikako Moriyoshi,[5] Takashi Suzuki,[4] Yoshihiro Kuroiwa,[5] and Dhananjai Pandey[1]

[1]*School of Materials Science and Technology, Indian Institute of Technology (Banaras Hindu University), Varanasi 221005, India*

[2]*Research and Technology Development Centre, Sharda University, Greater Noida 201306, India*

[3]*Forschungsneutronenquelle Heinz Maier-Leibnitz (FRM II), Technische Universität München, Lichtenbergstrasse 1, D-85747 Garching bei München, Germany*

[4]*Department of Quantum Matter, ADSM, Hiroshima University, Japan*

[5]*Department of Physical Science, Graduate School of Science, Hiroshima University, Japan*

(Received 12 May 2012; revised manuscript received 11 August 2012; published 30 November 2012)

The controversies about the structure of the true ground state of pseudorhombohedral compositions of $Pb(Zr_xTi_{1-x})O_3$ (PZT) are addressed using a 6% Sr^{2+} substituted sample with $x = 0.550$. Sound velocity measurements reveal a phase transition at $T_c \sim 279$ K. The temperature dependence of full width at half maximum of $(h00)_{pc}$ peaks and the unit cell volume also show anomalies around 279 K even though there is no indication of any change of space group in the synchrotron x-ray powder diffraction (SXRD) patterns. The neutron powder diffraction patterns reveal appearance of superlattice peaks below $T_c \sim 279$ K, confirming the existence of an antiferrodistortive phase transition. The Rietveld analysis of the room-temperature and low-temperature SXRD data below T_c shows that the structure corresponds to single monoclinic phase in the *Cm* space group while the analysis of neutron powder diffraction data reveals that the structure of the ground-state phase below T_c corresponds to the *Cc* space group. Our analysis shows that the structural models for the ground-state phase based on the *R3c* space group with or without the coexistence of the room-temperature monoclinic phase in the *Cm* space group can be rejected.

DOI: 10.1103/PhysRevB.86.174117 PACS number(s): 77.84.Cg, 61.05.cp, 61.05.fm, 77.80.B−

I. INTRODUCTION

Lead zirconate titanate $[Pb(Zr_xTi_{1-x})O_3]$, commonly known as PZT, is the most widely used piezoelectric ceramic in sensor and actuator devices.[1] It displays a rich and complex *x-T* phase diagram which contains a nearly vertical morphotropic phase boundary (MPB) at $x = 0.520$, a composition for which the piezoelectric and dielectric responses are highest.[1] The MPB has traditionally been believed to separate the stability fields of rhombohedral ($x > 0.520$) and tetragonal ($x < 0.520$) phases in the *R3m* and *P4mm* space groups, respectively.[1] In addition to the MPB, PZT shows two more phase boundaries on the Zr-rich side of the phase diagram. One such boundary occurs at $x \gtrsim 0.940$ and separates the stability field of an orthorhombic phase (space group *Pbam*) stable for $x \gtrsim 0.940$ from that of a second rhombohedral phase in the *R3c* space group. In this *R3c* phase, the oxygen octahedra are tilted about the trigonal axis[2] of the neighboring unit cells in an antiphase manner and, therefore, the structure belongs to the $a^-a^-a^-$ tilt system.[3] This rhombohedral phase with antiphase tilted octahedra results from a high-temperature rhombohedral phase with untilted octahedra in the *R3m* space group through an antiferrodistrotive (AFD) phase transition.[1] The AFD phase transition temperature first increases with decreasing Zr content, then peaks at $x \approx 0.850$, and, finally, starts decreasing until, for $x \approx 0.620$, the room-temperature phase corresponds to the *R3m* space group with untilted octahedra. This gives rise to another phase boundary at $x \approx 0.620$ separating the stability fields of the two different rhombohedral phases. All the phases (tetragonal *P4mm*, rhombohedral *R3m*, rhombohedral *R3c*, and orthorhombic *Pbam*) transform to the cubic paraelectric phase (*Pm3m*) and the corresponding transition temperature decreases with increasing Zr^{4+} content, irrespective of the structure of the room-temperature phase.

While the AFD phase transition in PZT has been well known since the phase boundary above room temperature between the "*R3m*" and "*R3c*" rhombohedral phases was established,[1] it was Ragini *et al.*[4] and Ranjan *et al.*[5] who discovered this transition below room temperature for compositions in the MPB region also, in agreement with a theoretical prediction by Fornari *et al.*[6] This discovery of the AFD transition below room temperature was subsequently confirmed by several researchers.[7–13] The phase below the AFD transition temperature is a superlattice phase of the higher-temperature phase.[4,5] The space group of this superlattice phase which also represents the ground state of PZT is currently under intense debate. To resolve this contentious issue, it is necessary to understand the subtle differences between three different types of monoclinic phases that exist or may exist at room temperature. (i) First, there is a pseudotetragonal monoclinic phase with the *Cm* space group for which the $(200)_{pc}$ peak is a doublet. As shown by Singh *et al.*[14] and Pandey *et al.*[15] using Rietveld analysis of high-resolution synchrotron x-ray powder diffraction (SXRD) data, this phase exists over a very narrow composition range, $0.520 \lesssim x < 0.530$, at room temperature, as confirmed by refinements. This is the phase discovered by Noheda *et al.*,[16,17] to which the tetragonal phase transforms below room temperature for $x = 0.520$. This phase exists in the vicinity of the MPB only and its stability field gets narrower with increasing temperature and undergoes an AFD transition to the superlattice phase below room temperature.[14,15] The space group of this monoclinic phase was first shown by Hatch *et al.*[18] to be *Cc*, which was subsequently confirmed by

others[11–13] but an alternative model based on the coexistence of $R3c + Cm$ phases has also been proposed by some workers.[8,9] (ii) Second, there is a pseudorhombohedral monoclinic phase also in the Cm space group for which the $(200)_{pc}$ is a singlet. The characteristic feature of this phase is anomalously large broadening of $(h00)_{pc}$ and $(hh0)_{pc}$ reflections, as was first pointed out by Ragini *et al.*[19] and subsequently confirmed by Singh *et al.*[14] in their high-resolution SXRD studies. Following Ragini *et al.*'s[19] work, other researchers have also accepted the assignment of Cm space group to such 'pseudorhombohedral' compositions.[20–24] The anomalous broadening of the $(h00)_{pc}$ and $(hh0)_{pc}$ reflections of the pseudorhombohedral monoclinic phase disappears in the tetragonal phase stable at $x < 0.520$.[19] This phase has been traditionally assigned the $R3m$ space group and is stable in the composition range $0.530 \leqslant x \leqslant 0.620$ in chemically homogeneous samples.[14,15,19] (iii) Third, there is a rhombohedral phase[1] or a pseudorhombohedral monoclinic phase[14,15] for $0.620 \lesssim x \lesssim 0.940$ which also exhibits anomalous broadening of the $(h00)_{pc}$ reflections but to a lesser extent as compared to the case for $0.530 \leqslant x \leqslant 0.620$. The powder XRD pattern of this rhombohedral or pseudorhombohedral phase contains superlattice peaks at room temperature due to the cell doubling caused by antiphase tilting of oxygen octahedra in the structure. Traditionally, this phase has been assigned the rhombohedral $R3c$ space group[1] but, according to Pandey *et al.*,[15] this phase may also be monoclinic in the Cc space group. The AFD transition temperatures for the first two types of monoclinic phases occur below room temperature[15] and decrease with decreasing Zr content, whereas for the third type it occurs above room temperature.[1] This suggests a weakening of the driving force for the AFD transition on approaching the MPB from the Zr-rich side. The AFD transition eventually disappears for tetragonal compositions away from the MPB.

To settle the Cc versus $R3c$ space group controversy for the ground state of pseudotetragonal monoclinic compositions of PZT, we recently[25] adopted a strategy combining the use of 6% Sr^{2+} substitution at Pb^{2+} site and high-wavelength neutrons (2.44 Å) to increase the tilt angle (and, hence, the intensity of the superlattice peaks) and separate the most intense lower angle superlattice peak at $q = (3/2\ 1/2\ 1/2)_{pc}$ from the neighboring intense $(111)_{pc}$ perovskite peak, respectively. Using these two strategies, we not only could resolve the intense $(3/2\ 1/2\ 1/2)_{pc}$ superlattice peak from the tail of the neighboring $(111)_{pc}$ peak but could also show that the $(3/2\ 1/2\ 1/2)_{pc}$ superlattice is not a singlet.[25] For the $R3c$ space group, this peak has to be a singlet. It was thus concluded that the space group of the pseudotetragonal composition of $(Pb_{0.94}Sr_{0.06})(Zr_xTi_{1-x})O_3$ (PSZT) for $x = 0.530$ is not $R3c$ but Cc.[25] As a next step, we consider in the present work AFD transition in a pseudorhombohedral monoclinic composition $(Pb_{0.94}Sr_{0.06})(Zr_{0.550}Ti_{0.450})O_3$ (PSZT550) with a view to settle the $R3c$-versus-Cc space group controversy for such compositions.[15,20–24] We present results of SXRD, neutron powder diffraction (NPD), and elastic modulus measurements which suggest that the $R3c$ space group can be rejected for the pseudorhombohedral compositions as well. We also compare the Rietveld refinement results for $R3c$ (including its coexistence with the Cm space group[15,25]) and Cc space group models for both the pseudotetragonal ($x = 0.530$, i.e., PSZT530) and pseudorhombohedral ($x = 0.550$, i.e., PSZT550) monoclinic compositions to settle the existing controversies about the space group of the ground state of PZT in and around the MPB region.

II. EXPERIMENT

Our samples were prepared by a semiwet route,[26] which is known to give the narrowest composition width $\Delta x \approx 0.01$ of the MPB region for pure PZT. A full description of the sample preparation was given in our previous work.[25] High-resolution SXRD measurements were carried out in the 100 K to 800 K temperature range at the BL02B2 beam line of SPring-8, Japan,[27] at a wavelength of 0.412 Å (30 keV). NPD data were obtained from FRMII, Germany, on the high-resolution SPODI[28] powder diffractometer at a wavelength of 2.536 Å. The longitudinal elastic modulus (C_L) was obtained by measuring the sound velocity (v) using the phase comparison-type pulse echo method.[29] Rietveld refinements using synchrotron and neutron powder diffraction data were carried out using the FULLPROF software package.[30]

III. RESULTS AND DISCUSSION

A. Room-temperature phase

Figure 1 depicts the SXRD profiles of the $(111)_{pc}$, $(200)_{pc}$, and $(220)_{pc}$ reflections at $T \leqslant 300$ K. For ease of discussion, we have also included in the figure the SXRD profiles of these reflections in the cubic phase at 800 K. For all temperatures with $T \leqslant 300$ K, the $(111)_{pc}$ and $(220)_{pc}$ are doublet, whereas

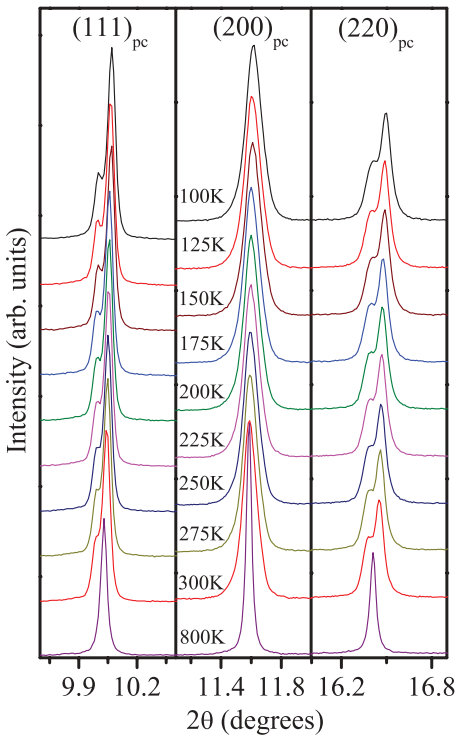

FIG. 1. (Color online) The evolution of synchrotron x-ray powder diffraction profiles of the $(111)_{pc}$, $(200)_{pc}$, and $(220)_{pc}$ reflections of PSZT550 with temperature.

$(200)_{pc}$ is a singlet, as expected for a rhombohedral structure. However, the $(200)_{pc}$ peak shows an anomalous broadening. The width of the $(200)_{pc}$ peak at $T = 300$ K is ~2.66 times that of the neighboring $(111)_{pc}$ peak. A similar anomalous broadening of $(h00)_{pc}$ peaks was reported by Ragini *et al.*[19] and Singh *et al.*[14] in the so-called rhombohedral compositions of PZT and Singh and Pandey[31] in PMN-xPT ceramics. The anomalous broadening of $(h00)_{pc}$-type reflections can be attributed to anisotropic strains which may result from the size difference between the Zr^{4+} and Ti^{4+} ions at the B site and/or Sr^{2+}/Pb^{2+} ions at the A site of the ABO_3 perovskite structure. It can also result from local compositional fluctuations. Anisotropic strain broadening can be modeled using Stephens's model[32] in the Rietveld refinements assuming the rhombohedral *R3m* space group. Unlike Frantti *et al.*[8] for $x = 0.530$ at room temperature and Zhang *et al.*[21] for $x = 0.60$ at 473 K, who considered the *R3c* space group for pseudorhombohedral compositions, we found no evidence to consider the *R3c* space group, as the superlattice reflections resulting from the $a^-a^-a^-$ oxygen octahedral tilt expected for this space group are not observed in the SXRD patterns. The intense superlattice peak $(3/2\ 1/2\ 1/2)_{pc}$ for the *R3c* space group is expected to occur at $d \approx 2.452$ Å in the SXRD data but no such peak is observed, as can be seen from Fig. 1(a) in the Supplemental Material.[33] The intensity of the $(3/2\ 1/2\ 1/2)_{pc}$ peak depends on small changes in the oxygen positions in the *R3c* space group with respect to those in the *R3m* space group. Since x rays cannot accurately detect such small changes in the positions of low-*Z* elements like oxygen, whereas the neutrons can locate the positions of oxygen atoms more accurately, we searched for the $(3/2\ 1/2\ 1/2)_{pc}$ superlattice peak in the neutron powder diffraction pattern also recorded at 300 K [see Fig. 1(b) in the Supplemental Material[33]]. But we found no evidence for this peak at room temperature even in the neutron diffraction pattern. Accordingly, the *R3c* space group model for PSZT550[8,21] can be rejected at room temperature, leaving behind the *R3m* space group as a plausible structural model.

We therefore refined the structure using the *R3m* space group considering all permitted anisotropic strain broadening parameters. The results are shown in Fig. 2(a), which reveals misfits for all $(hhh)_{pc}$, $(h00)_{pc}$, and $(hh0)_{pc}$ reflections, as can be seen from the inset. The value of χ^2 is 15.5, which is very high for a refinement to be crystallographically acceptable. It may, therefore, be concluded that the *R3m* space group cannot account for all the peaks consistently. On the other hand, consideration of the monoclinic space group *Cm* along with anisotropic strain broadening gave an excellent fit between the observed and calculated profiles, as can be seen from Fig. 2(b). The χ^2 dropped from a value of 15.5, for the best refinement using the *R3m* space group, to 2.95, for the *Cm* space group model, even though anisotropic strain broadening was considered in both cases. Yokota *et al.*[20] and Zhang *et al.*[21] have found for similar "pseudorhombohedral" compositions that a pure *Cm* space group cannot account for the observed diffraction profiles and they had to include a coexisting phase with the *R3m/R3c* space group in their refinements to obtain satisfactory Rietveld fits. Accordingly, we also considered the coexistence of two phases with *Cm* and *R3m* space groups in our refinements but the coexisting *R3m* phase was rejected in the refinement, giving a nearly zero phase fraction for this phase. This confirmed that our sample of PSZT550 is single-phase monoclinic in the *Cm* space group at 300 K. The refined parameters for the *Cm* space group are given in Table I of the Supplemental Material.[33] We believe that the coexisting phases reported by others[20–23,34] may essentially be the artifacts of chemical heterogeneities in the sample and are caused by the difference in the sample preparation technique.[35]

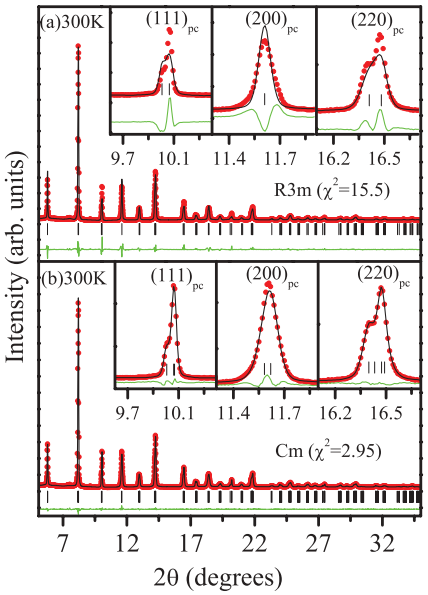

FIG. 2. (Color online) Observed (red dots), calculated (black continuous line), and difference (bottom line) profiles at 300 K using *R3m* and *Cm* space groups obtained after Rietveld refinement. The vertical tick marks above the difference profiles give the positions of the Bragg reflections. (Insets) The magnified view of Rietveld fits for selected $(111)_{pc}$, $(200)_{pc}$, and $(220)_{pc}$ reflections.

B. Low-temperature structural studies using SXRD

It is evident from Fig. 1 that there is no evidence for any additional peak splitting down to 100 K. Frantti *et al.*[8] and Yokota *et al.*[20] have proposed that the room-temperature monoclinic phase in the *Cm* space group undergoes an AFD transition to the rhombohedral phase in the *R3c* space group, even though the parent monoclinic phase continues to coexist with the rhombohedral phase at low temperatures. Since the superlattice reflections of the *R3c* space group are not discernible in the SXRD profiles of PSZT550, even at 100 K [see Fig. 2(a) of the Supplemental Material[33]] the *Cm*-to-*R3c* transition would appear as a Cm-to-*R3m* transition in the SXRD patterns. Accordingly, we refined the structure at 100 K using the SXRD data for the *R3m*, *R3m* + *Cm*, and *Cm* models. In all the refinements, anisotropic strain broadening was used. Figure 3(a) depicts the fits using the *R3m* model. It is evident from this figure that the *R3m* model does not explain the observed profiles as it leads to problems with fit and abnormally large χ^2 values, similar to the situation at 300 K. The consideration of the *Cm* model led not only to an excellent fit but also to a substantial reduction in the value of χ^2 from 20.4 (the best value that could be obtained for the *R3m* space group) to 2.91 at 100 K [see Fig. 3(b) for the Rietveld fit]. Attempts to carry out two-phase refinement using

the $R3m + Cm$ model of Frantti *et al.*[8] and Yokota *et al.*[20] was reduced to the Cm phase model, giving a zero phase fraction for the coexisting $R3m$ phase, as was the case at 300 K. Thus, SXRD data reveal no evidence for the Cm-to-$R3c/R3m$ or Cm-to-$R3c/R3m + Cm$ transition. We therefore can reject the proposition of the Cm-to-$R3m/R3c$ transition given in Refs. 8 and 20. Table I of the Supplemental Material[33] compares the refined parameters at 100 K with those at 300 K.

C. Indication of a phase transition at low temperatures

The Cm-to-$R3m/\ R3c + Cm$ or Cm-to-$R3m/R3c$ transition proposed in Refs. 8 and 20 is expected to be a first-order transition since $R3m$ is not a subgroup of the Cm space group. Accordingly, such a transition should lead to a small discontinuous change in the unit cell volume. The variation of unit cell volume of the monoclinic Cm phase, obtained by Rietveld refinement at various temperatures, is depicted in Fig. 4(a). This figure reveals no discontinuous change in the unit cell volume, suggesting the absence of any first-order transition below room temperature. However, there is a gradual change of slope around 270 K in Fig. 4(a). The linear interpolations from both the high- and low-temperature sides intersect at ∼275 K, suggesting that there may be a second-order phase transition around this temperature.

As pointed out earlier, since the full width at half maximum (FWHM) of $(200)_{pc}$ peak is ∼2.66 times that of the neighboring $(111)_{pc}$ peak, the structure could not be refined using the $R3m$ space group. If there is a Cm-to-$R3m$ phase transition below room temperature, one expects a decrease in the FWHM of the $(h00)_{pc}$ peaks. However, the FWHM of the $(h00)_{pc}$ peaks is found to increase with decreasing temperature, as shown in Fig. 4(b) for the $(200)_{pc}$ peak. Such an increase does not favor the rhombohedral $R3m$ space group. It is interesting to note that the FWHM increases nearly linearly from 400 K down to ∼275 K, beyond which it shows a quadratic dependence on temperature, indicating a phase transition around 275 K.

The existence of a phase transition at ∼275 K was confirmed by the observation of an anomaly in the temperature dependence of the elastic modulus of PSZT550 around 275 K. Figure 4(c) depicts the longitudinal elastic modulus (C_L) of PSZT550, obtained from ultrasonic velocity measurements as a function of temperature. The longitudinal elastic modulus decreases with decreasing temperature up to 279 K. Below 279 K, the longitudinal elastic modulus starts increasing. A decreasing value of the elastic modulus with decreasing temperature is anomalous and is a signature of lattice instability.[25] The fact that below 279 K the temperature dependence of C_L assumes normal behavior reveals a phase transition at $T_c \sim$ 279 K. The inset of Fig. 4(c) shows a magnified view of the transition region measured during heating and cooling cycles. The value of thermal hysteresis in T_c is less than 1 K, which suggests that this transition is of nearly second order or weakly first-order type.

D. Evidence for an AFD phase transition at low temperatures

Since the SXRD patterns reveal no structural change below $T_c \sim$ 275 K, around which we observe an anomaly in the unit cell volume, FWHM of $(h00)_{pc}$ peaks, and longitudinal elastic modulus, we collected neutron powder diffraction data on our sample in search of an AFD transition. Figures 2(a) and 2(b) of the Supplemental Material[33] depict the synchrotron x-ray and neutron powder diffraction patterns at 100 K,

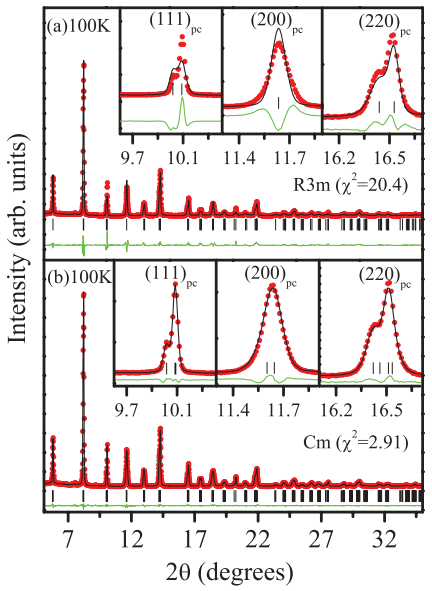

FIG. 3. (Color online) Observed (red dots), calculated (black continuous line), and difference (bottom line) profiles at 100 K using $R3m$ and Cm space groups obtained after Rietveld refinement. The vertical tick marks above the difference profiles give the positions of the Bragg reflections. (Insets) The magnified view of Rietveld fits for selected $(111)_{pc}$, $(200)_{pc}$, and $(220)_{pc}$ reflections.

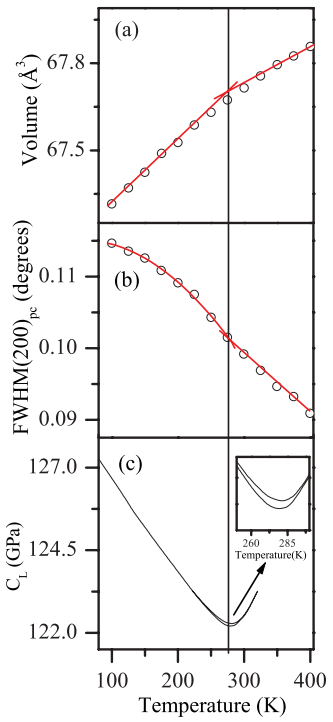

FIG. 4. (Color online) Temperature variation of (a) unit cell volume, (b) FWHM of the $(200)_{pc}$ peak, and (c) longitudinal elastic modulus (C_L) of PSZT550. [Inset of (c)] A magnified view of the phase transition region during heating and cooling cycles.

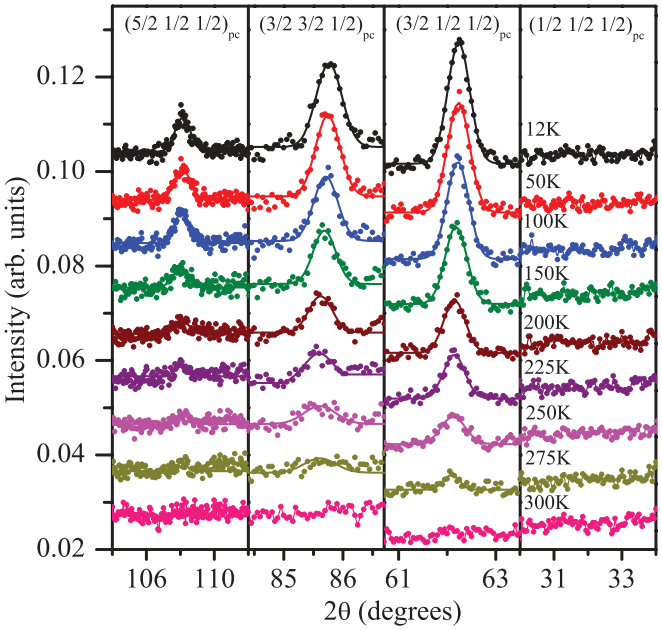

FIG. 5. (Color online) The evolution of neutron powder diffraction profiles of the $(3/2\ 1/2\ 1/2)_{pc}$, $(3/2\ 3/2\ 1/2)_{pc}$, and $(5/2\ 1/2\ 1/2)_{pc}$ superlattice reflections of PSZT550 as a function of temperature. (Intensities are normalized for comparison purposes and are plotted on the same scales.)

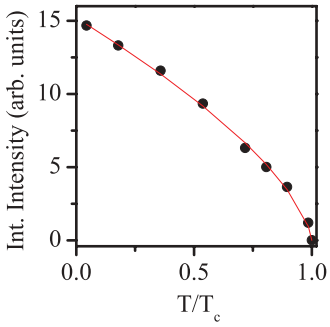

FIG. 6. (Color online) Variation in the integrated intensity of the $(3/2\ 1/2\ 1/2)_{pc}$ superlattice peak with temperature. Dots represent experimental values, while the continuous line corresponds to the least-squares fit for $I_{(3/2\,1/2\,1/2)pc} \sim (T_c - T)^{2\beta}$.

respectively. It is evident from this figure that new peaks with rather low intensities have appeared in the neutron powder diffraction pattern. All these peaks could be indexed as $(3/2\ 1/2\ 1/2)_{pc}$, $(3/2\ 3/2\ 1/2)_{pc}$, and $(5/2\ 1/2\ 1/2)_{pc}$ with respect to a pseudocubic cell. The presence of peaks with such odd-odd-odd half-integer indices suggests an AFD transition leading to the antiphase rotation of the oxygen octahedra in the neighboring unit cells[3] which are driven by phonon instabilities at the $q = (1/2\ 1/2\ 1/2)_{pc}$ point of the cubic Brilloun zone. The evolution of the intensity of the three superlattice peaks due to the AFD transition is depicted in Fig. 5 for the temperature range from 12 K to 300 K. It is evident from this figure that all superlattice peaks disappear above 275 K, in agreement with the appearance of an anomaly in the longitudinal elastic modulus, unit cell volume, and FWHM of $(h00)_{pc}$ peaks. While we observe the $(3/2\ 1/2\ 1/2)_{pc}$, $(3/2\ 3/2\ 1/2)_{pc}$, and $(5/2\ 1/2\ 1/2)_{pc}$ superlattice peaks, the $(1/2\ 1/2\ 1/2)_{pc}$ superlattice peak is not discernible (see the last column in Fig. 5). This aspect is discussed later on.

The tilt angle associated with an AFD transition constitutes the order parameter whose temperature dependence can be studied by investigating the temperature dependence of the integrated intensity of the superlattice peak, which is proportional to the square of the tilt angle. Figure 6 depicts the temperature dependence of the integrated intensity of the pseudocubic $(3/2\ 1/2\ 1/2)$ superlattice reflection. The solid line gives the least-squares fit for the power law $I_{(3/2\,1/2\,1/2)pc} \sim (T_c - T)^{2\beta}$, for which an exponent of 0.326 and $T_c \backsimeq 279$ K was determined. The value of the exponent is close to 1/3. Such a value has been reported in the past by Muller and Berlinger[36] for the *I4/mcm*-to-$Pm\bar{3}m$ AFD transition in $SrTiO_3$ and $R\bar{3}c$-to-$Pm\bar{3}m$ AFD transition in $LaAlO_3$ using electron paramagnetic resonance (EPR) measurements. They showed that the order parameter follows second-order behavior with $\beta = 1/2$ for $T/T_c \lesssim 0.9$ but, in the narrow $0.9 < T/T_c < 1.0$ temperature range, it deviates from $\beta = 1/2$ and becomes $\beta = 1/3$. They attributed it to the breakdown of the mean-field behavior near T_c. However, the situation in Fig. 6 differs, as it does not show linear dependence above $T/T_c \sim 0.9$. We therefore were constrained to fit the power-law dependence, $I_{(3/2\,1/2\,1/2)pc} \sim (T_c - T)^{2\beta}$, over the entire temperature range. This fitting gave us $\beta = 1/3$ and $T_c \sim 279$ K. In recent years such a value of $\beta = 1/3$ has been argued to be due to near tricritical behavior[37,38] within the mean-field approximation.

E. Structure of the ground state of PSZT550

The superlattice peaks appearing at and below $T_c \sim 275$ K in the neutron powder diffraction patterns may be due to *R3c* or *Cc* space groups,[8,11–13,15,18,20–24] as discussed earlier. We analyzed the neutron diffraction data at 12 K using *R3c*, $R3c + Cm$, and *Cc* space group models. Figure 7 compares the Rietveld fits of $(200)_{pc}$, $(220)_{pc}$, and $(111)_{pc}$ perovskite peaks for these three models. The fits for the three prominent superlattice peaks $(3/2\ 1/2\ 1/2)_{pc}$, $(3/2\ 3/2\ 1/2)_{pc}$, and $(5/2\ 1/2\ 1/2)_{pc}$ are shown in Fig. 8. It is evident from Fig. 7(a) that the *R3c* space group cannot account for the intensity of the main perovskite reflections satisfactorily. Consideration of the coexisting *Cm* phase, as proposed by Frantti *et al.*[8] and Yokota *et al.*,[20] improves the fits and χ^2 drops from 8.37 to 5.50, as can be seen from Fig. 7(b). The results of refinement using the *Cc* space group are shown in Fig. 7(c). The *Cc* space group leads to a significant improvement in the fits. The χ^2 (2.81) for the *Cc* space group is significantly lower than that for the $R3c + Cm$ phase coexistence model (5.50). Further, the *R3c* or the $R3c + Cm$ coexistence model cannot account for the $(5/2\ 1/2\ 1/2)_{pc}$ superlattice peak, as shown in Fig. 8. The calculated peak position for the best Rietveld fit using *R3c* or $R3c + Cm$ models is shifted towards lower angles with respect to the observed peak position. Also, the calculated profile shape cannot explain the observed profile shape of the $(5/2\ 1/2\ 1/2)_{pc}$ peak. Such a misfit in the peak position of $(5/2\ 1/2\ 1/2)_{pc}$ superlattice peak was also pointed out earlier by Ranjan *et al.*[39] for pure PZT with $x = 0.520$. The *Cc* space group model, in contrast to the *R3c* or $R3c + Cm$ models, not

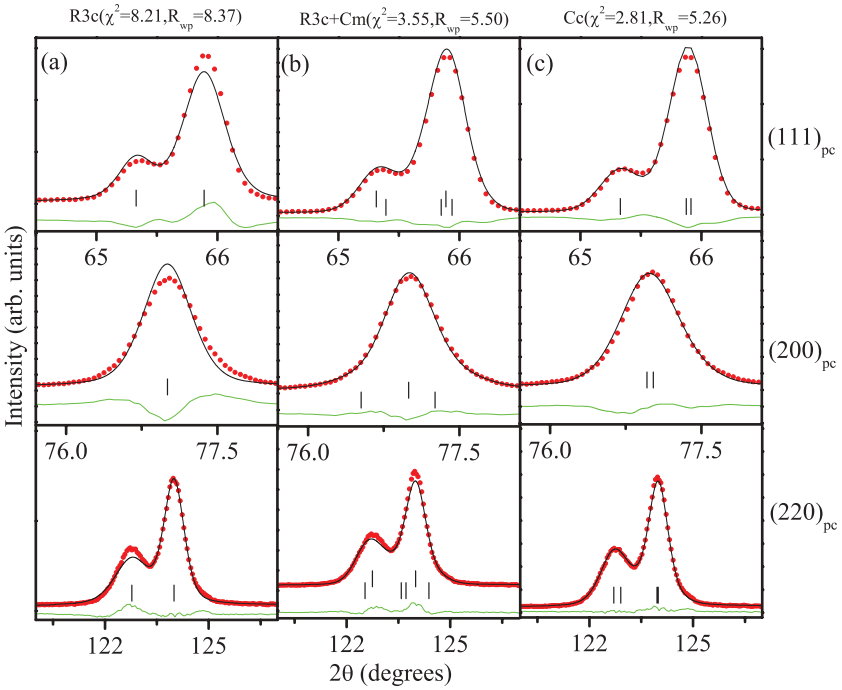

FIG. 7. (Color online) Observed (red dots), calculated (black continuous line), and difference (bottom line) plots of the three perovskite peaks $(111)_{pc}$, $(200)_{pc}$, and $(220)_{pc}$ of PSZT550 at 12 K, as obtained by Rietveld refinement using (a) *R3c*, (b) $R3c + Cm$, and (c) *Cc* structural models.

only accounts for the $(5/2\ 1/2\ 1/2)_{pc}$ superlattice peak but also gives better fits for all other peaks, the main perovskite as well as the superlattice peaks. It is worth mentioning here that the number of refinable parameters for the $R3c + Cm$ model (43) is higher than that (35) for the *Cc* model and yet it is the *Cc* model which gives lower χ^2 and overall excellent fit. All these factors obviously favor the *Cc* space group. Figure 3 of the Supplemental Material[33] gives the overall fit using the *Cc* model for PSZT550. Table I gives the coordinates of the atoms in the *Cc* phase, as obtained by the refinement.

The *Cc* space group also permits a $(1/2\ 1/2\ 1/2)_{pc}$ superlattice peak which is otherwise extinguished for the *R3c* space group. The last row of Fig. 8 shows the Rietveld refined pattern around the $q = (1/2\ 1/2\ 1/2)_{pc}$ position for all three models. It is evident from this figure that the intensity of the calculated pattern using the *Cc* structural model for the $(1/2\ 1/2\ 1/2)_{pc}$ superlattice reflection is within the background counts of the neutron diffraction pattern. The peak intensity is about 0.096% of the strongest $(111)_{pc}$ perovskite reflection in the neutron diffraction pattern. Evidently, this reflection is not discernible due to the extremely low intensity (smaller structure factor).

As stated earlier, even the stronger superlattice reflections present in the neutron powder diffraction patterns are not discernible in the SXRD patterns. We simulated the x-ray powder diffraction pattern using the lattice parameters and coordinates obtained from Rietveld refinement of neutron diffraction data (see Fig. 4 of the Supplemental Material[33]) for PSZT550 at 100 K. The inset of this figure shows a magnified view of the superlattice $(3/2\ 1/2\ 1/2)_{pc}$ along with some part of the perovskite $(111)_{pc}$ reflection. It is evident from the inset that the intensity of this peak is within the background counts and, hence, cannot be discernible. The intensity of $(3/2\ 1/2\ 1/2)_{pc}$ superlattice reflection in the simulated pattern for x rays is about 0.1% of the strongest $(110)_{pc}$ perovskite reflection, which is comparable to the intensity of the $(1/2\ 1/2\ 1/2)_{pc}$ peak (0.096%) in the neutron powder diffraction pattern. The intensities of the other superlattice reflections, $(3/2\ 3/2\ 1/2)_{pc}$ and $(5/2\ 1/2\ 1/2)_{pc}$, are found to be still weaker. Our simulations thus suggest that the absence of all the

TABLE I. Refined structural parameters and agreement factors for PSZT550 using neutron powder diffraction data at 12 K with the *Cc* space group.

$T = 12$ K, *Cc* space group $a = 10.0316(2)$ Å, $b = 5.7462(2)$ Å, c = 5.7748(2) Å, $\beta = 125.637(2)$ $\chi^2 = 2.32$, $R_{wp} = 4.76$				
Atoms	*x*	*y*	*z*	*B* (Å^2)
Pb/Sr	0	0.75	0	$\beta_{11} = 0.001(1)$, $\beta_{22} = 0.00$, $\beta_{33} = 0.007(2)$, $\beta_{12} = 0.005(1)$, $\beta_{13} = 0.0058(8)$, $\beta_{23} = 0.013(1)$
Ti/Zr	0.219(5)	0.253(6)	0.247(3)	0.02(3)
O1	−0.029(1)	0.270(2)	0.370(3)	0.81(3)
O2	0.219(1)	0.520(2)	0.0373(3)	0.19(1)
O3	0.205(1)	−0.007(2)	0.500(1)	0.33(2)

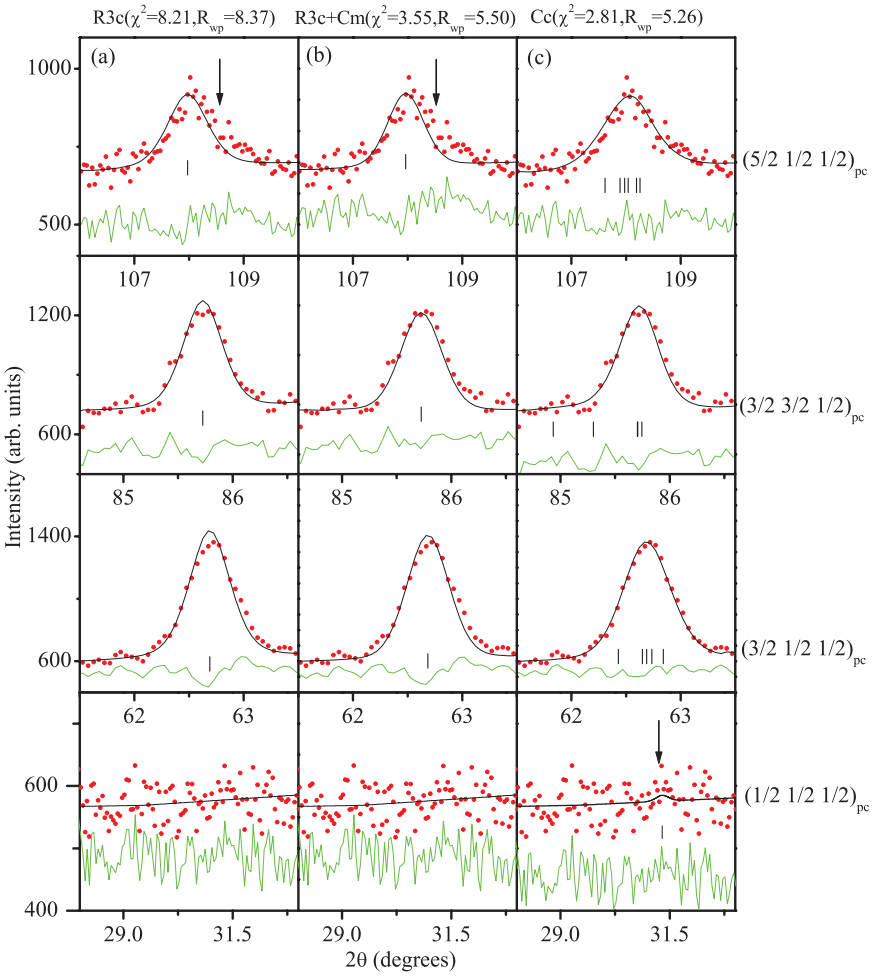

FIG. 8. (Color online) Observed (red dots), calculated (black continuous line), and difference (green bottom line) plots of the three superlattice peaks $(3/2\ 1/2\ 1/2)_{pc}$, $(3/2\ 3/2\ 1/2)_{pc}$, and $(5/2\ 1/2\ 1/2)_{pc}$ of PSZT550 at 12 K, as obtained by Rietveld refinement using (a) *R3c*, (b) *R3c* + *Cm*, and (c) *Cc* structural models.

superlattice reflections in the SXRD patterns and the $(1/2\ 1/2\ 1/2)_{pc}$ superlattice reflection in the powder neutron diffraction pattern have a common origin, i.e., extremely low intensity.

F. Comparison with the *Cc* space group for PSZT530 composition

From the large asymmetry and nonsinglet nature of the $(3/2\ 1/2\ 1/2)_{pc}$ superlattice peak, we concluded in our previous work[25] on PSZT with $x = 0.530$ (a pseudotetragonal composition) that the *R3c* space group for which the $(3/2\ 1/2\ 1/2)_{pc}$ reflection should be a singlet can be rejected. However, the results of Rietveld refinements for the *R3c* and *R3c* + *Cm* models were not given in our earlier work.[25] In order to understand the difference in the shape of the profiles and their Reitveld fits for various superlattice reflections of PSZT530 and PSZT550, we present in Fig. 9 the observed, calculated, and difference profiles of PSZT530. It is evident from this figure that the calculated peak position of the $(3/2\ 1/2\ 1/2)_{pc}$ superlattice reflection is significantly shifted away from the observed peak position for the *R3c* and *R3c* + *Cm* structural models. In the case of PSZT550, because of the pseudorhombohedral character of the monoclinic phase at room temperature and below, the $(3/2\ 1/2\ 1/2)_{pc}$ peak is nearly symmetric and, therefore, we do not see a huge mismatch between the calculated and observed peak positions of the $(3/2\ 1/2\ 1/2)_{pc}$ superlattice peak of PSZT550, as is evident from a comparison of fits given in Fig. 9 and Fig. 8. However, the *R3c* as well as the *R3c* + *Cm* structural models lead to a significant mismatch between the observed and calculated profiles of the $(5/2\ 1/2\ 1/2)_{pc}$ superlattice peak in both PSZT530 and PSZT550, although the mismatch is more pronounced in PSZT530 than in PSZT550. The discrepancies in the fits for the *R3c* and *R3c* + *Cm* models disappear for the Cc structural model, suggesting clearly that both the pseudotetragonal (PSZT530) and pseudorhombohedral (PSZT550) monoclinic phases at room temperature transform, respectively, to low-temperature pseudotetragonal and pseudorhombohedral superlattice phases, which have the same space group, *Cc*.

IV. CONCLUDING REMARKS

The results presented in this and the previous work[25] conclusively establish that the ground-state phase of PSZT for both the pseudotetragonal ($x = 0.530$) and pseudorhombohedral ($x = 0.550$) monoclinic compositions are pseudotetragonal and pseudorhombohedral monoclinic, respectively, both having the same *Cc* space group. The two compositions considered by us correspond to inside ($x = 0.530$) and outside ($x = 0.550$) the MPB region. The alternative models based on *R3c* + *Cm* or only the *R3c* space groups lead to a pronounced discrepancy between the observed and calculated profiles, especially for the superlattice peaks. However, this discrepancy

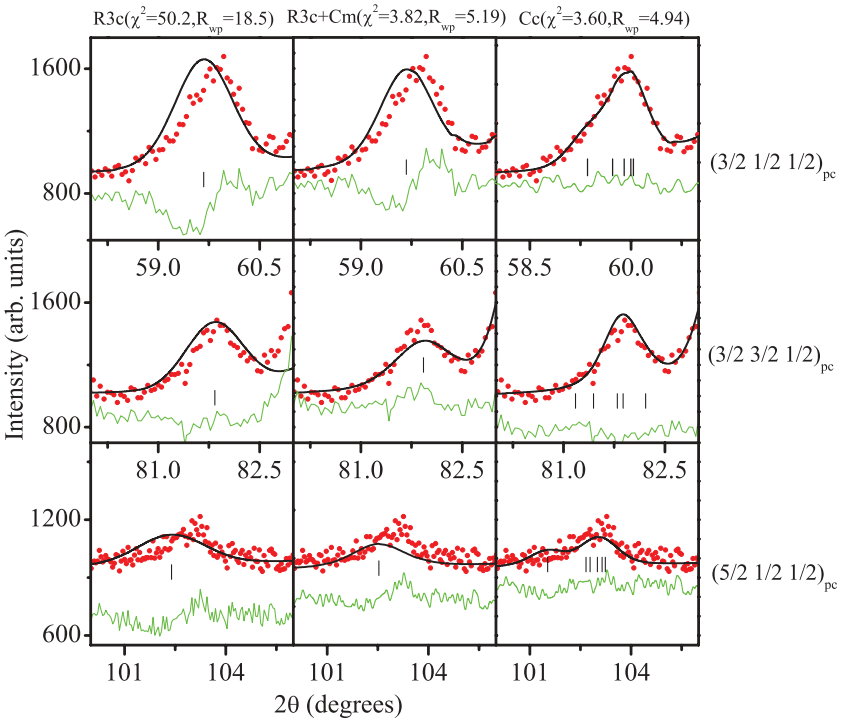

FIG. 9. (Color online) Observed (red dots), calculated (black continuous line), and difference (bottom line) plots of three superlattice reflections $(3/2\ 1/2\ 1/2)_{pc}$, $(3/2\ 3/2\ 1/2)_{pc}$, and $(5/2\ 1/2\ 1/2)_{pc}$ obtained by Rietveld refinement of PSZT530 using (i) *R3c*, (ii) *R3c* + *Cm*, and (iii) *Cc* structural models. The vertical tick marks above the difference profiles give the positions of the Bragg reflections.

decreases with increasing Zr^{4+} content as one moves away from the pseudotetragonal monoclinic compositions towards the pseudorhombohedral monoclinic compositions. This is evident from a comparison of Fig. 8 with Fig. 9. It is, therefore, imperative to use pseudorhombohedral compositions as close to the MPB as possible to distinguish between the rhombohedral (*R3c*) and monoclinic (*Cc*) structural models for an unambiguous determination of the ground-state superlattice phase of PSZT and, for that reason, of PZT also. The conclusions arrived at by Yokota *et al.*[20] in favor of the *R3c* + *Cm* structural model are based on the Rietveld analysis of diffraction data for compositions with $0.60 \leqslant x \leqslant 0.92$ which are far away from the MPB. Moreover, it may not be easy to distinguish between the rhombohedral and monoclinic superlattice models on the basis of the mismatch between the observed and calculated profiles of the superlattice peaks. However, the anomalous broadening of the $(h00)_{pc}$ peaks is still present for such Zr^{4+}-rich compositions (see Fig. 8 of Ragini *et al.*[19] and Fig. 3 of Singh *et al.*[14]). Pandey *et al.*[15] have shown that this anomalous broadening can be explained better using the *Cc* space group than the *R3c* space group.

The main objection against the *Cc* space group is the nonobservation of a peak at the $q = (1/2\ 1/2\ 1/2)_{pc}$ position, which is extinguished for the *R3c* space group but is permitted by the *Cc* space group. It may be noted that the calculated intensity of the $(1/2\ 1/2\ 1/2)_{pc}$ superlattice peak (~0.096% of strongest intensity $(111)_{pc}$ perovskite reflection for PSZT550 in neutron diffraction pattern) is rather too low to be observable above the background level. Further, the nonobservation of this extremely low-intensity peak in neutron powder diffraction data is as enigmatic as the nonobservation of the rather intense superlattice reflections (in neutron diffraction patterns) at the $q = (3/2\ 1/2\ 1/2)_{pc}$, $(3/2\ 3/2\ 1/2)_{pc}$, and $(5/2\ 1/2\ 1/2)_{pc}$ positions in synchrotron x-ray powder diffraction patterns. We showed that the calculated intensities of these nonobservable superlattice peaks in the SXRD patterns is $\leqslant 0.1\%$, which is comparable to the intensity of the nonobservable $(1/2\ 1/2\ 1/2)_{pc}$ superlattice peak in the neutron powder patterns. It was because of the nonobservation of the intense superlattice peaks in the SXRD patterns that Noheda *et al.*[16] missed the superlattice phase, discovered later by Ragini *et al.*[4] and Ranjan *et al.*,[5] in their first set of experiments at 20 K, and erroneously concluded that the space group for the ground state phase of PZT in the MPB region is *Cm*.

Based on the analysis of the observed superlattice peaks, we conclude that the structural models for the ground-state phase of PZT based on the *R3c* space group with or without the consideration of the coexistence of the room-temperature monoclinic phase in the *Cm* space group can be rejected and that the space group of the ground state of PZT corresponding to the compositions in the MPB and on the Zr^{4+}-rich side of the MPB is *Cc*.

ACKNOWLEDGMENTS

R. S. Solanki acknowledges financial support from Council of Scientific and Industrial Research (CSIR), India. D. Pandey and Y. Kuroiwa acknowledge financial support from the Department of Science and Technology (DST), Government of India, and the Japan Society for the Promotion of Science (JSPS) of Japan under the Indo-Japan Science Collaboration Program. The synchrotron radiation experiments were performed at the BL02B2 beamline of Spring-8 with the approval of the Japan Synchrotron Radiation Research Institute (Proposals No. 2011A1324 and No. 2011A0084). T. Suzuki and I. Ishii thank [the Grant-in-Aid for Scientific Research on Innovative Areas "Heavy Electrons" (No. 20102005)] the Ministry of Education, Culture, Sports, Science and Technology of Japan for support.

[1]B. Jaffe, W. R. Cook, and H. Jaffe, *Piezoelectric Ceramics* (Academic Press, London, 1971), p. 135.
[2]C. Michel, J.-M. Moreau, G. D. Achenbach, R. Gerson, and W. J. James, Solid State Commun. **7**, 865 (1969).
[3]A. M. Glazer, Acta Crystallogr. Sect. B **28**, 3384 (1972); Acta Crystallogr. Sect. A **31**, 756 (1975).
[4]Ragini, S. K. Mishra, D. Pandey, Herman Lemmens, and G. Van Tendeloo, Phys. Rev. B **64**, 054101 (2001).
[5]Rajeev Ranjan, Ragini, S. K. Mishra, D. Pandey, and B. J. Kennedy, Phys. Rev. B **65**, 060102(R) (2002).
[6]M. Fornari and D. J. Singh, Phys. Rev. B **63**, 092101 (2001).
[7]B. Noheda, L. Wu, and Y. Zhu, Phys. Rev. B **66**, 060103(R) (2002).
[8]J. Frantti, S. Ivanov, S. Eriksson, H. Rundlof, V. Lantto, J. Lappalainen, and M. Kakihana, Phys. Rev. B **66**, 064108 (2002); J. Frantti, J. Phys. Chem. B **112**, 6521 (2008).
[9]A. M. Glazer, P. A. Thomas, K. Z. Baba-Kishi, G. K. H. Pang, and C. W. Tai, Phys. Rev. B **70**, 184123 (2004).
[10]I. A. Kornev, L. Bellaiche, P.-E. Janolin, B. Dkhil, and E. Suard, Phys. Rev. Lett. **97**, 157601 (2006).
[11]D. I. Woodward, J. Knudsen, and I. M. Reaney, Phys. Rev. B **72**, 104110 (2005).
[12]D. E. Cox, B. Noheda, and G. Shirane, Phys. Rev. B **71**, 134110 (2005).
[13]J. Rouquette, J. Haines, V. Bornand, M. Pintard, Ph. Papet, W. G. Marshall, and S. Hull, Phys. Rev. B **71**, 024112 (2005).
[14]A. K. Singh, D. Pandey, S. Yoon, S. Baik, and N. Shin, Appl. Phys. Lett. **91**, 192904 (2007).
[15]D. Pandey, A. K. Singh, and S. Baik, Acta Crystallogr. Sect. A **64**, 192 (2008).
[16]B. Noheda, D. E. Cox, G. Shirane, J. A. Gonzalo, L. E. Cross, and S.-E. Park, Appl. Phys. Lett. **74**, 2059 (1999).
[17]B. Noheda, J. A. Gonzalo, L. E. Cross, R. Guo, S.-E. Park, D. E. Cox, and G. Shirane, Phys. Rev. B, **61**, 8687 (2000).
[18]D. M. Hatch, H. T. Stokes, Rajeev Ranjan, Ragini, S. K. Mishra, D. Pandey, and B. J. Kennedy, Phys. Rev. B **65**, 212101 (2002).
[19]Ragini, R. Ranjan, S. K. Mishra, and D. Pandey, J. Appl. Phys. **92**, 3266 (2002).
[20]H. Yokota, N. Zhang, A. E. Taylor, P. A. Thomas, and A. M. Glazer, Phys. Rev. B **80**, 104109 (2009).
[21]N. Zhang, H. Yokota, A. M. Glazer, and P. A. Thomas, Acta Crystallogr. Sect. B **67**, 386 (2011).
[22]D. Phelan, X. Long, Y. Xie, Z.-G. Ye, A. M. Glazer, H. Yokota, P. A. Thomas, and P. M. Gehring, Phys. Rev. Lett. **105**, 207601 (2010).
[23]S. Gorfman, D. S. Keeble, A. M. Glazer, X. Long, Y. Xie, Z.-G. Ye, S. Collins, and P. A. Thomas, Phys. Rev. B **84**, 020102(R) (2011).
[24]Guillaume Fraysse, Julien Haines, Véronique Bornand, Jérôme Rouquette, Marie Pintard, Philippe Papet, and Steve Hull, Phys. Rev. B **77**, 064109 (2008).
[25]R. S. Solanki, A. K. Singh, S. K. Mishra, S. J. Kennedy, T. Suzuki, Y. Kuroiwa, C. Moriyoshi, and D. Pandey, Phys. Rev. B **84**, 144116 (2011).
[26]A. P. Singh, S. K. Mishra, D. Pandey, Ch. D. Prasad, and R. Lal, J. Mater. Sci. **28**, 5050 (1993).
[27]E. Nishibori, M. Takata, K. Kato, M. Sakata, Y. Kubota, S. Aoyagi, Y. Kuroiwa, M. Yamakata, and N. Ikeda, Nucl. Instrum. Methods A **467-468**, 1045 (2001).
[28]M. Hoelzel, A. Senyshyn, R. Gilles, H. Boysen, and H. Fuess, Neutron News **18**, 23 (2007).
[29]T. Goto, T. Suzuki, A. Tamaki, Y. Ohe, S. Nakamura, and T. Fujimura, *The Bulletin of the Research Institute for Scientific Measurement* (Tohoku University, Sendai, Japan, 1989), Vol. 38, p. 65.
[30]J. Rodriguez-Carvajal Laboratory, FULLPROF, a Rietveld and pattern matching and analysis program, version July 2011, Laboratoire Leon Brillouin, CEA-CNRS, France [http://www.ill.eu/sites/fullprof/].
[31]A. K. Singh, D. Pandey, and O. Zaharko, Phys. Rev. B **68**, 172103 (2003).
[32]P. W. Stephens, J. Appl. Crystallogr. **32**, 281 (1999).
[33]See Supplemental Material at http://link.aps.org/supplemental/10.1103/PhysRevB.86.174117 for (i) a comparison of synchrotron x-ray and neutron powder diffraction patterns at 300 K and 100 K, (ii) Rietveld fit for neutron powder diffraction pattern at 12 K, (iii) calculated/simulated SXRD patterns at 100 K, and (iv) refined structural parameters and agreement factors obtained after Rietveld analysis of SXRD data at 300 K and 100 K.
[34]R. G. Burkovsky, Yu. A. Bronwald, A. V. Filimonov, A. I. Rudskoy, D. Chernyshov, A. Bosak, J. Hlinka, X. Long, Z.-G. Ye, and S. B. Vakhrushev, Phys. Rev. Lett. **109**, 097603 (2012).
[35]A. P. Wilkinson, J. Xu, S. Pattanaik, and S. J. L. Billinge, Chem. Mater. **10**, 3611 (1998).
[36]K. A. Muller and W. Berlinger, Phys. Rev. Lett. **26**, 13 (1971).
[37]E. K. H. Salje, J. Mc Jimenz Gallardo, F. J. Romero, and J. del Cerro, J. Phys.: Condens. Matter **10**, 5535 (1998).
[38]S. K. Mishra and D. Pandey, Phys. Rev. B **79**, 174111 (2009).
[39]R. Ranjan, A. K. Singh, Ragini, and D. Pandey, Phys. Rev. B **71**, 092101 (2005).